Bridging Multiferroic Phase Transitions by Epitaxial Strain in $BiFeO_3$

I. C. Infante,[1] S. Lisenkov,[2] B. Dupé,[3] M. Bibes,[1] S. Fusil,[1] E. Jacquet,[1] G. Geneste,[3,4] S. Petit,[5] A. Courtial,[6] J. Juraszek,[6] L. Bellaiche,[7] A. Barthélémy,[1,*] and B. Dkhil[3,†]

[1]*Unité Mixte de Physique CNRS/Thales, 1 avenue Fresnel, Campus de l'Ecole Polytechnique, 91767 Palaiseau, France and Université Paris-Sud, 91405 Orsay, France*

[2]*Department of Physics, University of South Florida, Tampa, Florida 33647, USA*

[3]*Laboratoire Structures, Propriétés et Modélisation des Solides, UMR CNRS-Ecole Centrale Paris, Grande Voie des Vignes, 92295 Châtenay-Malabry Cedex, France*

[4]*CEA, DAM, DIF, F-91297 Arpajon, France*

[5]*Laboratoire Léon Brillouin, CEA/CNRS UMR12, 91191 Gif-sur-Yvette, France*

[6]*Groupe de Physique des Matériaux, UMR CNRS 6634, Université de Rouen, 76801 St Etienne du Rouvray, France*

[7]*Physics Department, University of Arkansas, Fayetteville, Arkansas 72701, USA*

(Received 16 April 2010; published 28 July 2010)

We report the influence of epitaxial strain on the multiferroic phase transitions of $BiFeO_3$ films. Using advanced characterization techniques and calculations we show that while the magnetic Néel temperature hardly varies, the ferroelectric Curie temperature T_C decreases dramatically with strain. This is in contrast with the behavior of standard ferroelectrics where strain enhances the polar cation shifts and thus T_C. We argue that this is caused by an interplay of polar and oxygen tilting instabilities and that strain can drive both transitions close together to yield increased magnetoelectric responses.

DOI: 10.1103/PhysRevLett.105.057601 PACS numbers: 77.55.Nv, 75.85.+t, 77.80.bn, 85.75.−d

Strain engineering [1] has recently emerged as a powerful way to tune the various remarkable physical properties [2,3] of ABO_3 perovskite oxide thin films. While epitaxial strain controls the Néel temperature T_N in antiferromagnetic (AFM) films by modifying oxygen octahedral tilt angles [4], it usually enhances the Curie temperature T_C for ferroelectric films by increasing polar cation shifts [5].

Among multiferroic perovskite oxides, $BiFeO_3$ (BFO) is the most studied because both polar and magnetic orders coexist at room temperature. Below the Curie temperature $T_C \approx 1100$ K, bulk BFO is described by the rhombohedral $R3c$ space group that allows antiphase octahedral tilting and ionic displacements from the centrosymmetric positions about and along the same [111] pseudocubic direction, respectively. In addition to the G-type antiferromagnetic spin ordering, a cycloid-type spatial spin modulation occurs below the Néel temperature $T_N \approx 640$ K [6].

The highly multifunctional nature of BFO and its parenthood with other strain-sensitive perovskites have triggered much effort to engineer its physical properties through strain. However and quite disappointingly, it is now established that neither polarization [7–10] nor room-temperature magnetic properties vary much with strain [11,12], except for the appearance of a weak magnetic moment in strained films [13]. On the other hand, the consequences of misfit strains on the *transition temperatures* have been poorly addressed. This is surprising, as bringing the magnetic and ferroelectric transition temperatures closer together, for instance through biaxial stresses, would offer an original approach to design materials with enhanced magnetoelectric responses [14].

In this Letter, we report the strain dependence of the ferroic transition temperatures in a series of epitaxial BFO thin films. The films were grown by pulsed laser deposition on several substrates [15], namely, $(LaAlO_3)_{0.3}$-$(Sr_2AlTaO_6)_{0.7}$ (LSAT), $SrTiO_3$ (STO), $DyScO_3$ (DSO), $GdScO_3$ (GSO), $SmScO_3$ (SSO), and $NdScO_3$ (NSO), having in-plane (IP) average parameters ranging from 3.880 Å for LSAT to 4.006 Å for NSO. Such a variety of substrates allows a virtually continuous change of the IP misfit strain $\varepsilon_{in} = (a_{av} - a_{bulk})/a_{bulk}\%$ (with a_{av} being the average pseudocubic IP parameter of the substrate and a_{bulk} being the pseudocubic parameter of BFO). To avoid structural relaxation, the BFO thickness was set to 70 nm for all samples expect for those grown on LSAT for which it was 35 nm. For Mössbauer spectroscopy experiments, similar samples were grown using a ~100% ^{57}Fe-enriched BFO target. To measure the ferroelectric properties, fully strained bottom electrodes of either $La_{2/3}Sr_{1/3}MnO_3$ (LSMO)—for LSAT and STO—or $SrRuO_3$ (SRO)—for DSO, GSO, SSO, and NSO—were inserted between BFO and the substrate.

Figure 1 shows the results of room-temperature x-ray diffraction (XRD) measurements. From Fig. 1(a) we infer that BFO grows single phase and epitaxially along the $[001]_C$ direction on all substrates. Figs. 1(b)–1(e) display a selection of equivalent pseudocubic $(103)_C$ XRD reciprocal-space mappings for BFO on STO [Fig. 1(b)], DSO [Fig. 1(c)], GSO [Fig. 1(d)], and NSO [Fig. 1(e)] that we use to quantify the strain state. Remarkably, the peaks for the substrate and film present identical $q_{\|}$ (IP reciprocal-space unit), thus attesting that BFO is fully strained on all the substrates. The extracted out-of-plane (OP) c parameter as a function of the IP misfit strain clearly follows a linear dependence [see Fig. 1(f)], indicating an elastic deformation of the BFO unit. Thus, using this series

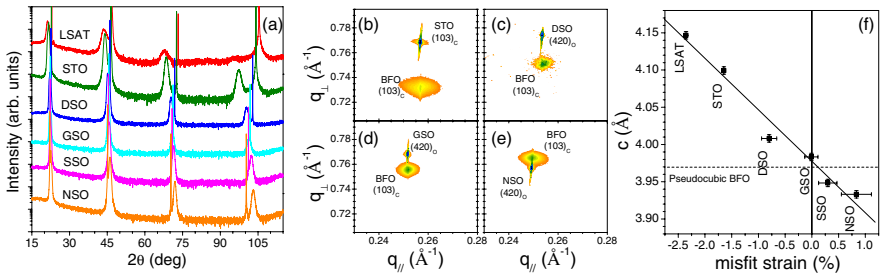

FIG. 1 (color online). (a) θ–2θ scans of BFO films grown on different substrates. (b)–(e) Reciprocal-space maps of BFO films grown on STO (b), DSO (c), GSO (d), and NSO (e). (f) Room-temperature OP parameter c as a function of the measured in-plane strain of BFO films grown on different substrates. Horizontal error bars include the difference in the IP parameter along $[001]_O$ and $[1\ -10]_O$ directions for $[110]_O$-oriented substrates.

of substrates, a large variation of IP strain values has been achieved, from compressive -2.4% to tensile $+0.9\%$.

Because BFO thin films are clamped in the plane, all structural changes resulting from thermal expansion and phase transitions are accommodated through variations of the OP lattice parameter. Therefore, to study the role of strain on phase transitions, we measured the temperature evolution of the OP c parameter using the $(002)_C$ substrate and film peaks. The temperature dependences of the OP parameters of BFO films, $c_{\mathrm{FE\ film}}$, and those of the corresponding substrates, c_{subst}, are plotted in Figs. 2(a)–2(f). While the OP substrate parameter shows the classical linear thermal expansion behavior, $c_{\mathrm{FE\ film}}$ exhibits, at a substrate-dependent specific temperature, an inflection point that signals a phase transformation [16]. To get a better quantitative determination of this transition, the thermal expansion contribution (as provided by the purely paraelectric OP parameter $c_{\mathrm{PE\ film}}$) has been evaluated and subtracted from the experimental data of $c_{\mathrm{FE\ film}}$ [17]. Figures 2(g)–2(l) display $\Gamma(T)$ defined as $\Gamma(T) = [c_{\mathrm{FE\ film}}(T)\text{-}c_{\mathrm{PE\ film}}(T)]/c_{\mathrm{FE\ film}}(300\ \mathrm{K})$ that reflects the ferroelectric order parameter. Following a mean field approach, the experimental data in Figs. 2(g)–2(l) have been fitted [see solid lines in Figs. 2(g)–2(l)] to a general function $\Gamma(T) = A + B(T_C - T)^{1/2}$, where A and B are constants and T_C is the ferroelectric Curie temperature of the considered film. One can see that the highest T_C is obtained for BFO on SSO [$\sim$1200 K, Fig. 2(k)], and that the Curie temperature of the other BFO films drops with respect to that of the BFO bulk. In the case of the film grown on LSAT [$T_C \sim 740$ K, Fig. 2(g)], T_C is $\sim$360 K lower than in the bulk. Strikingly, the stronger the compressive strain, the lower the T_C value. Such findings are very surprising and unexpected because (i) in all known conventional ferroelectric perovskite films T_C increases (rather than strongly decreases) when increasing the magnitude of the compressive or tensile strain [5,18–21] and (ii) they are in contradiction with recent predictions of transition temperatures in BFO films [22].

To directly study the ferroelectric transition and confirm its anomalous strain dependence we performed temperature-dependent piezoresponse microscopy (PFM), proceeding as follows. We first poled the BFO heterostructures, imaged them at room temperature, annealed them in a pure oxygen atmosphere during $2h$ at a target temperature, and reinspected the poled regions by PFM at 300 K. As visible in Figs. 3(a) and 3(b), the OP contrast and stripe shape progressively disappear as the annealing temperature is increased. The PFM signals degrade at a lower temperature for BFO/LSMO//LSAT compared to BFO/SRO//DSO and, after heating to 923 K, the most highly strained BFO/LSMO//LSAT sample presents partially erased domains, whereas all poled stripes remain for the BFO/SRO/DSO sample. After annealing at 1023 K, a weak but measurable OP phase contrast is measured for BFO/SRO//DSO while no stripe is observed for BFO/LSMO//LSAT. This is even more visible from the averaged profiles also displayed in Figs. 3(a) and 3(b).

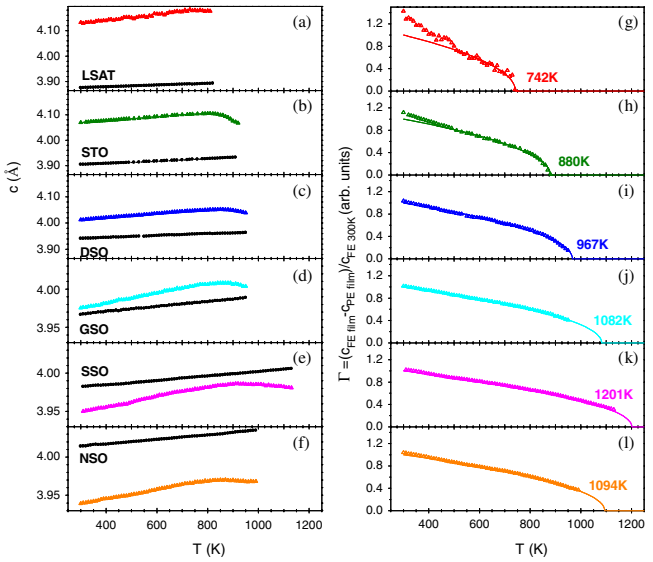

FIG. 2 (color online). (a)–(f) OP parameter of BFO films (triangles) and the different substrates (circles) in pseudocubic notation. (g)–(l) Normalized OP parameter of BFO films (after correction of the paraelectric OP contribution) (symbols) and corresponding mean field fits (lines). Data shown in this figure correspond to samples grown on LSAT (a),(g), STO (b),(h), DSO (c),(i), GSO (d),(j), SSO (e),(k), and NSO (f),(l).

Note that after coming back to room temperature after the high temperature process, new stripes could still be written indicating that the loss of PFM contrast at high temperature was not due to film decomposition [bottom of Figs. 3(a) and 3(b)]. Although this experimental procedure is believed to overestimate the true T_C, because the induced polarization is metastable and decays with time [23], these results confirm that T_C shows an unexpected decrease with compressive strain, in agreement with XRD.

To determine T_N, we performed Mössbauer spectroscopy and neutron diffraction experiments as a function of temperature. The Mössbauer spectra of the BFO//GSO film at 298 and 530 K are presented in Fig. 3(c) (top and bottom, respectively). In the AFM state the Mössbauer spectra can be approximated by two six-line spectra with different hyperfine fields [24] that progressively decrease in temperature. The fitting of the hyperfine field evolution in a mean field theory allows us to deduce T_N [Fig. 3(d)], which in this case is around 640 K. In Fig. 3(e), we display the $(\frac{1}{2}\,\frac{1}{2}\,\frac{1}{2})_C$ reflection related to the G-type AFM ordering of the BFO//STO film. The peak persists up to the maximum temperature achieved in this experiment (623 K) that

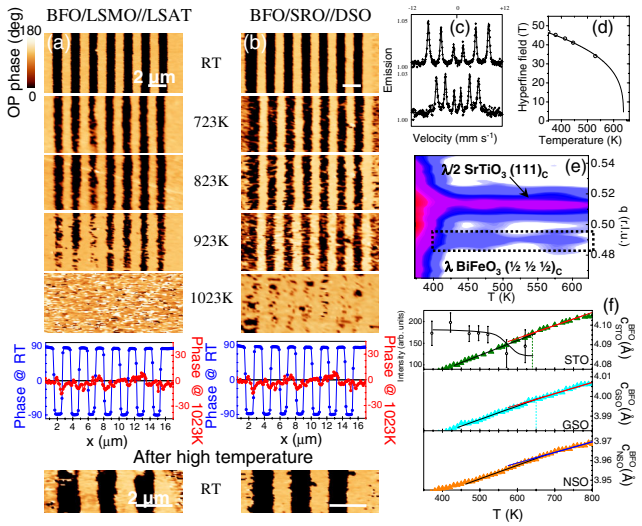

FIG. 3 (color online). OP phase piezoresponse images measured after poling for BFO/LSMO//LSAT (a) and BFO/SRO//DSO (b) at room temperature (RT) (top) and after annealing 723, 823, 923, and 1023 K, and corresponding averaged phase profiles perpendicular to stripes obtained at RT (blue triangle) and 1023 K (red circles). Bottom: Rewritten artificial domains after annealing. (c) Mössbauer spectra of the BFO//GSO film at 298 K (top) and 530 K (bottom). (d) Corresponding hyperfine field evolution (symbols) as a function of temperature together with the mean field fit (line). (e) AFM peak $(\frac{1}{2}\,\frac{1}{2}\,\frac{1}{2})_C$ as a function of temperature measured using neutron diffraction on a 400 nm BFO film on STO. The evolution of the peak intensity is reported in (f), the line is a guide for the eyes. (f) OP c parameter as a function of temperature of BFO films on STO, GSO, and NSO. Changes in slope, signaled by the linear fits, indicate the second order transition from an AFM to a paramagnetic state at T_N.

is close to the bulk T_N (~640 K). We fitted the AFM peak intensity dependence in temperature to evaluate T_N [Fig. 3(f), open symbols], which we estimate to be $T_N > 575$ K [25]. Interestingly, this AFM transition is also visible in the XRD data. In Fig. 3(f) (filled symbols) we include the temperature behaviors of the OP c parameter around 640 K for BFO films on STO, GSO, and NSO. The change of slope of the temperature evolution of the c- parameter [linear fits in Fig. 3(f)] indicates that a phase transition occurs closely to the corresponding bulk T_N. Clearly, the film T_N values are weakly affected, if at all, by the compressive strain, in contrast with the strong effects observed on the ferroelectric transition.

To reach a deep understanding of the strain dependence of the ferroic transition temperature, we have also investigated $[001]_C$-oriented epitaxial BFO films from a first-principles-based effective Hamiltonian method [26]. In order to compare experimental and theoretical data, we have recalculated the misfit strain of BFO films calculating the IP misfit strain ε_{in} at the T_C rather than at room temperature [as in Fig. 1(f)]. Therefore, in Fig. 4, we used $\varepsilon_{\text{in}} = [a_{\text{av}}(T = T_{C\,\text{film}}) - a_{\text{bulk}}(T_{C\,\text{film}})]/a_{\text{bulk}}(T_{C\,\text{film}})\%$. Experimental film T_C values were deduced from XRD data, and the unit cell parameters of bulk BFO $a_{\text{bulk}}(T)$ have already been reported [27]. Figure 4(c) displays the critical temperature-versus-misfit-strain diagram (lines), as predicted by the effective Hamiltonian, along with the measured T_C (circles) and T_N (squares and triangle). A very good qualitative and quantitative agreement is obtained between theory and experiment, indicating that while T_N is mostly independent of strain and close to its bulk value, T_C drastically decreases with increasing compressive IP strain and tetragonality [c/a ratio, Fig. 4(a)]. This unexpected result is numerically found to originate from the enhancement of the antiferrodistortive angle along the z axis (ω_Z) under compressive strain [blue line in Fig. 4(b)], likewise causing an increase of the critical temperature at which a purely antiferrodistortive paraelectric state occurs [T_{001}, black line in Fig. 4(c)]. In other words, the tilting of oxygen octahedra, and its interaction with ferroelectricity, is responsible for the anomalous strain dependence of T_C in BFO films in contrast with conventional ferroelectrics (such as $BaTiO_3$ or $PbTiO_3$) where the increase of the misfit strain results in an increase of the c/a and a consecutive increase of T_C. Thus, neglecting the antiferrodistortive degree of freedom, which does not exist in conventional ferroelectrics, leads to an incorrect phase diagram for BFO films [22]. Interestingly, such tilting and especially its response to strain and its coupling with electric dipoles open a new way to *simultaneously* optimize many physical properties [18]. In particular, it allows T_C to get closer to T_N, by applying a compressive strain, which naturally results in large piezoelectric and dielectric responses, huge magnetic susceptibility, and a dramatic enhancement of cross-coupling effects (such as magnetoelectric coefficients) below T_N [28].

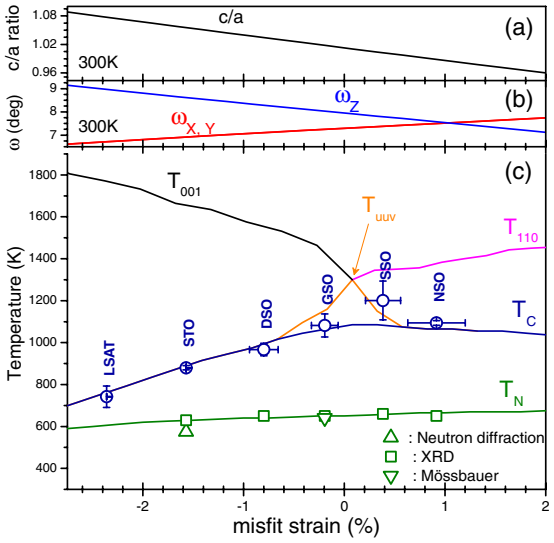

FIG. 4 (color online). Effective Hamiltonian results evaluated in a BFO film, at 300 K and as a function of misfit strain, (a) tetragonality (c/a ratio), and (b) antiferrodistortive angles ω along x, y, and z axes (ω_X and ω_Y, red line, and ω_Z, blue line). (c) Theoretical results on BFO film transition temperatures (T_C, blue line, and T_N, green line) as a function of misfit strain. The activation temperatures for the antiferrodistortive oxygen tilting along the z direction (tetragonal distortion T_{001}, black line), for the antiferrodistortive oxygen tilting within the x-y plane (orthorhombic distortion T_{110}, red line), and for the tilting along $[uuv]$ direction (monoclinic distortion T_{uuv}, orange line) are also plotted. Experimental T_C (circles) and T_N (squares and triangles) values. Vertical error bars for T_N values correspond to symbol size and for T_C values result from maximum variation of T_C that may be obtained between different fitting processes using the mean field function. Below T_C, for any considered strain, the simulations predict that the crystallographic phase is Cc, with a polarization along a $[uuv]$ direction while the oxygen octahedra rotate about a $[u'u'v']$ axis.

In summary, we combined theoretical and experimental investigation on BFO thin films that evidence the anomalous behavior of their transition temperatures under strain. As a matter of fact, T_N is virtually independent of strain, while T_C strongly decreases under compressive strain in BFO films (in contrast with conventional ferroelectric thin films). This latter unexpected result arises from a competition between polar displacements and the often neglected oxygen octahedra tilts. Our original findings therefore open a novel route for designing efficient magnetoelectric devices by tuning their critical temperatures, in general, and bringing them closer together, in particular. They also shed light into the need of adopting a new and comprehensive view that incorporates oxygen tilts and their interactions with other physical properties of multiferroic compounds.

We thank P.-E. Janolin for fruitful discussions, P. Bonville for experimental support, D. Colson for providing the BFO targets, and K. Peters from Crystec GmbH. This work was supported by the EU STREP Macomufi, the French C-Nano Ile-de-France Magellan, the French PRES Universud Nano-Ox, the French ANR Pnano, the ONR Grants No. N00014-04-1-0413, No. N00014-08-1-0915, and No. N00014-07-1-0825, NSF Grants No. DMR 0701558 and No. DMR-0080054, and DOE Grant No. DE-SC0002220, and the University of South Florida. Some computations were made possible thanks to the MRI Grant No. 0722625 and to the HPCMO of the DOD.

*agnes.barthelemy@thalesgroup.com
†brahim.dkhil@ecp.fr

[1] D. G. Schlom *et al.*, Annu. Rev. Mater. Res. **37**, 589 (2007).
[2] Y. Tokura and N. Nagaosa, Science **288**, 462 (2000).
[3] E. Dagotto, Science **309**, 257 (2005).
[4] J. W. Seo *et al.*, J. Phys. Condens. Matter **20**, 264014 (2008).
[5] K. J. Choi *et al.*, Science **306**, 1005 (2004).
[6] G. Catalan and J. F. Scott, Adv. Mater. **21**, 2463 (2009).
[7] C. Ederer and N. Spaldin, Phys. Rev. Lett. **95**, 257601 (2005).
[8] H. N. Lee *et al.*, Phys. Rev. Lett. **98**, 217602 (2007).
[9] B. Dupé *et al.*, Phys. Rev. B **81**, 144128 (2010).
[10] H. Béa *et al.*, Phys. Rev. Lett. **102**, 217603 (2009).
[11] W. Eerenstein *et al.*, Science **307**, 1203a (2005).
[12] H. Béa *et al.*, Phys. Rev. B **74**, 020101(R) (2006).
[13] H. Béa, M. Bibes, S. Petit, J. Kreisel, and A. Barthélémy, Philos. Mag. Lett. **87**, 165 (2007).
[14] H. Schmid, Ferroelectrics **162**, 317 (1994).
[15] H. Béa *et al.*, Appl. Phys. Lett. **87**, 072508 (2005).
[16] Previous XRD experiments (not shown) have shown that BFO films may decompose at a temperature higher than 1100 K. This is why almost all our XRD data shown in Fig. 2 are limited to 1000 K in order to insure the preservation of the film quality.
[17] We extracted $c_{\text{PE film}}$ using the OP strain ε_{out}, as $\varepsilon_{\text{out}} = (c_{\text{PE film}} - a_{\text{PE bulk}})/a_{\text{PE bulk}} = 2\nu_{\text{film}}\varepsilon_{\text{int}}/(\nu_{\text{film}} - 1)$ with ν_{film} the Poisson coefficient, $a_{\text{PE bulk}}$ the bulk pseudocubic BFO parameter extrapolated from Ref. [27], and the IP strain $\varepsilon_{\text{int}} = (a_{\text{subst}} - a_{\text{PE bulk}})/a_{\text{PE bulk}}$, assuming that the IP parameters are clamped to that of the substrate (a_{subst}). Therefore, $c_{\text{PE film}}(T) = a_{\text{PE bulk}}(T) + 2\nu_{\text{film}}[a_{\text{subst}}(T) - a_{\text{PE bulk}}(T)]/(\nu_{\text{film}} - 1)$.
[18] E. Bousquet *et al.*, Nature (London) **452**, 732 (2008).
[19] E. D. Specht, H.-M. Christen, D. P. Norton, and L. A. Boatner, Phys. Rev. Lett. **80**, 4317 (1998).
[20] N. Yanase, K. Abe, N. Fukushima, and T. Kawakubo, Jpn. J. Appl. Phys. **38**, 5305 (1999).
[21] M. Dawber *et al.*, Adv. Mater. **19**, 4153 (2007).
[22] R. J. Zeches *et al.*, Science **326**, 977 (2009).
[23] J. E. Spanier *et al.*, Nano Lett. **6**, 735 (2006).
[24] J. De Sitter *et al.*, Solid State Commun. **18**, 645 (1976).
[25] Near $(\frac{1}{2}\,\frac{1}{2}\,\frac{1}{2})_C$ BFO peak (from λ), the structural $(111)_C$ STO peak appeared (from $\lambda/2$) because of maximized neutron beam flux.
[26] I. A. Kornev *et al.*, Phys. Rev. Lett. **99**, 227602 (2007).
[27] R. Haumont *et al.*, Phys. Rev. B **78**, 134108 (2008).
[28] J. C. Wojdel and J. Iñiguez, Phys. Rev. Lett. **105**, 037208 (2010).